Catalysis Science & Technology

PAPER

View Article Online
View Journal | View Issue

Cite this: *Catal. Sci. Technol.*, 2015, 5, 1919

Palladium nanoparticles confined in thiol-functionalized ordered mesoporous silica for more stable Heck and Suzuki catalysts†

Rafael L. Oliveira,[a] Wuliyasu He,[a] Robertus J. M. Klein Gebbink[b] and Krijn P. de Jong*[a]

Received 18th November 2014,
Accepted 31st December 2014

DOI: 10.1039/c4cy01517g

www.rsc.org/catalysis

Palladium nanoparticles of similar size of ~2 nm were synthesized on different silica-based materials, all functionalized with thiol groups *i.e.*, Aerosil-380, SBA-15, plugged SBA-15 and m-MCF. The resulting materials were used to study the influence of the confinement of Pd nanoparticles in a functionalized silica support on the Heck and the Suzuki reactions. In the case of the Heck reaction, for all catalysts it was proven that leached Pd species were responsible for the activity. However, the catalysts based on ordered mesoporous silica were still able to restrict Pd particle growth, giving rise to an enhanced stability. For the Suzuki reaction, stronger alkaline conditions were required and catalysts based on plugged SBA-15 showed a higher stability than those based on SBA-15 and m-MCF, which both collapsed after the first cycle. At almost identical Pd particle size, ordered mesoporous materials enhance stability and particle growth is slowed down but not fully suppressed.

Introduction

Ordered mesoporous silica (OMS) such as SBA-15 and MCM-41 has attracted increased interest in the last two decades because of its unique properties such as controllable pore size, large internal surface area and narrow pore size distribution. Due to these properties, numerous applications of OMS in different fields have been reported such as sensors,[1–3] drug delivery systems,[4–6] chromatography[7,8] and catalysis.[9–16] In catalysis, however, siliceous materials do not have sufficient intrinsic activity and a lot of effort has been done to introduce active species in their pores such as organometallic complexes, molecules with alkaline and acidic properties and metal particles.[17–20]

Silica has been used as a support to many different metal nanoparticles.[21–26] However, OMS has been found to be very interesting because of the possibility to study the effect of the confinement of nanoparticles on their stability. Hao *et al.* compared the catalytic activity of gold nanoparticles immobilized on SBA-16 and commercial silica gel for the oxidative esterification of alcohols, concluding that the cages of SBA-16 were efficient to prevent the growth of Au; as a consequence, Au/SBA-16 showed a longer lifetime.[27] Prieto *et al.* observed the same phenomena for methanol synthesis using Zn promoted Cu nanoparticles immobilized on SBA-16 and silica gel.[28] In another example, Sun *et al.* proved that silver nanoparticles confined in SBA-15 have a higher thermal stability than particles immobilized on the silica gel surface.[29]

Despite the vast literature about mesoporous materials in catalysis, these materials face big limitations, *i.e.* their limited mechanical and hydrothermal stability. Many efforts have been done to produce OMS with a higher stability, for example, Kisler *et al.* functionalized the MCM-41 surface with alkyl groups and proved that its hydrothermal stability increased significantly.[30] Pham *et al.* coated the SBA-15 structure with a thin carbon film and reported that the synthesized material has a higher hydrothermal stability than SBA-15.[31] Van der Voort *et al.* modified the SBA-15 synthesis and produced a new material called plugged SBA-15; this material showed a higher mechanical and thermal stability when compared to other OMS, due to the pillaring effect.[32–34]

Plugged SBA-15 was synthesized using an excess of tetraethyl orthosilicate (TEOS), the silica precursor, leading to an ordered mesoporous silica with constricted pores. By varying the synthesis parameters, the extent of plugging can be influenced. Further studies on plugged SBA-15 showed that entrance sizes and cavity length can be tuned by changing the synthetic parameters.[35,36] Another interesting OMS is the modified mesocellular foam (m-MCF) that was recently synthesized by Shakeri *et al.*[37] The procedure is based on P-SBA-15 synthesis, but in this case they introduced a swelling agent

[a] *Inorganic Chemistry and Catalysis, Debye Institute for Nanomaterials Science, Utrecht University, Netherlands. E-mail: k.p.dejong@uu.nl*
[b] *Organic Chemistry and Catalysis, Debye Institute for Nanomaterials Science, Utrecht University, Netherlands*

† Electronic supplementary information (ESI) available. See DOI: 10.1039/c4cy01517g

(mesitylene) during the synthesis which caused the formation of larger cages. Some of the very interesting characteristics of this material are its narrow entrance sizes and large cages. Moreover, they also showed using electron tomography that the cages are connected with 9–12 neighboring cavities, resulting in a highly interconnected network.

Palladium nanoparticles have been widely immobilized on different supports and have been applied as catalysts for many reactions such as oxidation, reduction, C–C cross coupling and others;[38–47] among C–C coupling reactions, the Suzuki and the Heck reactions are the most explored examples. However, Pd nanoparticles immobilized on inorganic matrices often suffer from leaching and particle growth due to Ostwald ripening, resulting in a limited recyclability in most cases.[48–51] Recently, a lot of work has been done to produce more efficient heterogeneous catalysts for C–C cross coupling reactions. For examples, Pagliaro *et al.* entrapped Pd nanoparticles using a sol–gel procedure, producing leach-proof nanostructures; these materials could be recycled seven times without losing activity.[52] Budroni *et al.* also entrapped Pd nanoparticles in a sponge-like silica and reported that leached species were partially responsible for the conversion.[53] Park *et al.* immobilized Pd nanoparticles on silica nanotubes, producing efficient nano-reactors for the Suzuki reaction, and they reported an insignificant Pd leaching and concluded the surface nature of the Suzuki reaction.[54]

A lot of reports in the literature have shown that supports with functional groups containing sulfur, nitrogen, or phosphorous can lead to more stable catalysts for C–C cross coupling.[55–61] Recently, our group reported that SBA-15 with thiol grafted on its surface produced a more stable catalyst than Pd immobilized on bare SBA-15.[62] In another example, Ma *et al.* used an ionic liquid to stabilize palladium nanoparticles on the SBA-15 surface. They reported a higher stability of this material when compared with Pd impregnated on pristine SBA-15.[63]

In this contribution, Pd nanoparticles of almost the same size were synthesized on different silica supports, *i.e.*, Aerosil-380, SBA-15, plugged SBA-15, and m-MCF, all modified with thiol ligands. These materials were used to study the effect of the confinement of functionalized silica on the activity and the recyclability of the Heck and the Suzuki reactions. The leaching of Pd, growth of Pd particles and stability of silica supports were examined to explain the possible reasons for the deactivation of the catalysts.

Experimental

Synthesis and catalytic performance

Chemicals. Triblock copolymer poly(ethylene oxide)-poly(propylene oxide)-poly(ethylene oxide) (P123), tetraethyl orthosilicate (99%), (3-mercaptopropyl)-triethoxysilane (80%), 2% cross-linked poly(4-vinylpyridine) (PVPy), butyl acrylate (99%), triethylamine (99%), tetraamminepalladium(II) nitrate solution (10 w/w% in water and 5 wt% Pd on carbon (product number 20568-0)) were purchased from Sigma-Aldrich. Palladium acetate ($Pd(OAc)_2$, 47.1% Pd) and Aerosil-380 were purchased from Degussa, and iodobenzene (98%), 4-iodoanisole (98%) and *n*-butylamine (99%) were purchased from Acros Organics.

Ordered mesoporous silica. SBA-15 and plugged SBA-15 (hereafter referred to as P-SBA-15) were synthesized following a procedure previously described.[36]

For m-MCF synthesis, 4 grams of copolymer Pluronic P123 was dissolved in an aqueous acidic solution (150 ml; 1.6 M) in a 500 mL polypropylene bottle at room temperature overnight. Then, 3 grams of TMB (mesitylene) was added to the reaction mixture at 35 °C dropwise and stirred vigorously for 2 h. After this period, 17 grams of TEOS was slowly added to the mixture (1.5 mL min^{-1}) and stirred vigorously for 5 minutes. After this period, the mixture was kept under static conditions at 35 °C for 20 hours followed by 24 hours at 80 °C. The solid product was collected by filtration, washed with distilled water, dried at 60 °C for 24 h and calcined at 550 °C in static air for 6 hours.

Functionalization of silica surface. 500 mg of SBA-15, P-SBA-15, m-MCF and Aerosil-380 was dried at 140 °C under vacuum for 12 hours. After this, the solid was dispersed in 20 mL of dried toluene under nitrogen. Then, 2.0 mL of (3-thiopropyl)triethoxysilane (MPTES) was added to the mixture dropwise over 5 minutes under vigorous stirring. Then, the mixture was heated at 110 °C and stirred for 24 hours under nitrogen. The obtained materials were filtered off, washed once with toluene and twice with ethanol, and dried at 60 °C for 24 hours.

Aerosil-380 was also functionalized using a different methodology. In this procedure, 500 mg of silica was dried at 140 °C as previously described. Then, the silica was dispersed in 20 mL of dried toluene. Then, 300 μL of glacial CH_3COOH and 1.5 mL of MPTES were added subsequently to the reaction mixture dropwise. The mixture was allowed to react at 110 °C under N_2 for 24 hours. The solid was collected and washed as previously described.

Impregnation of Pd. 250 mg of functionalized silica support was dried under vacuum at 140 ° C for 12 hours. After drying, the solid was dispersed in 5 mL of dry toluene under N_2. 8 mg of palladium(II) acetate was dissolved in 1 mL of dichloromethane and then added slowly to the dispersion. The dispersion was then heated to 60 °C and stirred for 24 h. The solids were collected by centrifugation, washed once with toluene and once with ethanol, and finally dried at 60 °C. For reduction of palladium, 100 mg of Pd-loaded silica was dispersed in 1 mL of water. Then, 1 mL of 0.1 M $NaBH_4$ was added rapidly under vigorous stirring. After 20 minutes, the dispersion was diluted with water to 35 mL, centrifuged, washed thoroughly with water and dried at 60 °C under stagnant air.

Catalyst tests

The Heck reaction. In a typical Heck reaction, a mixed solution of iodobenzene (2.25 mmol), butyl acrylate (3.47 mmol), NEt_3 (2.15 mmol), hexamethylbenzene (internal standard for GC analysis, 1.1 mmol), 2.0 mL of toluene and 0.2 mL of

DMF was added in a Schlenk tube, followed by addition of 20 mg of catalyst (0.1 mol% palladium relative to iodobenzene). Then, the mixture was stirred for a given time and temperature.

After the reaction, solid catalysts were recovered by centrifugation, washed with ethanol (35 mL) and dried under vacuum. For recycling experiments, a new solution mixture, as described above, was added to the solid.

The Suzuki reaction. In a typical reaction, a mixed solution of 4-iodoanisole (2.4 mmol), phenylboronic acid (2.88 mmol), base (2.4 mmol,) and solvent (4 mL) was added in a Schlenk tube, followed by addition of 20 mg of catalyst (0.1 mol% palladium relative to 4-iodoanisole). Then, the mixture was allowed to react at a desired temperature and time. For the recycle experiment, the catalyst was recovered by centrifugation and the solid was washed with ethanol/water (1/1, 2 × 40 mL) and ethanol (30 mL) and then dried at 60 °C overnight. Then, a new solution mixture, as described above, was added to the solid and allowed to react for the same period of time. As just one product was observed, the conversions were obtained by external calibration.

GC analysis. A small fraction of the liquid samples was taken, diluted with toluene and analyzed by GC-FID. CG analysis was performed using a PerkinElmer Clarus 500, equipped with a 30 m capillary column with 5% phenyl/95% methylpolysiloxane as the stationary phase (AT5), using the following parameters: initial temperature 50 °C, temperature ramp 10 °C min^{-1}, final temperature 250 °C, injection volume 0.5 μL.

Hot filtration test and PVPy poison test. A Heck reaction was allowed to run for 3 hours for a mixture of solvents. Then, the solids were filtered off under static vacuum using a swivel frit filter connected with an empty flask; the filtrate was kept at reaction temperature, and the conversion was monitored by GC.

The catalyst poison was added to the Schlenk flask before the addition of the reaction solution. Poly(4-vinylpyridine) (2% cross-linked) (PVPy) was used in 350 equivalents of pyridine sites to the total of palladium.

Characterization

Electron microscopy. The morphology and sizes of the silica particles were determined with a Tecnai FEI XL 30SFEG Scanning Electron Microscope (SEM). Transmission electron microscopy was performed using a FEI Tecnai20F microscope, operating at 200 kV and equipped with a CCD camera.

The samples were embedded in epoxy resin (Epofix, EMS) and cured at 60 °C overnight. Then, they were cut into thin sections with a nominal thickness of 60 nm using a Diatome Ultra knife, 4 mm wide and 35° clearance angle, mounted on a Reichert–Jung Ultracut E microtome. The sections floating on water after cutting were picked up, deposited onto a carbon coated polymer grid and left to dry. The histograms of the particle size distribution were obtained from observing about 500 particles in representative micrographs of different areas.

Gas physisorption. N_2 and Ar physisorption measurements were performed at 77 K using a Micromeritics Tristar 3000. The samples were dried before the measurement under a N_2 flow at 250 °C for at least 12 h. The functionalized samples were dried at 130 °C for at least 12 h. The total microporous and mesoporous volume (V_p) was determined using the *t*-plot method. The pore size distribution of the mesoporous silica supports was calculated from the adsorption branch of the isotherm by BJH analysis. The maximum of the pore size distribution was taken as the average pore diameter.

XRD analysis. Long range pore ordering was confirmed by low-angle X-ray diffraction. Patterns were obtained at room temperature from 0.5 to 8° 2θ with an AXS D2 Phaser powder X-ray diffractometer, in Bragg–Brentano mode, equipped with a Lynxeye detector using Co Kα_{12} radiation, with λ = 1.790 Å, operating at 30 kV and 10 mA. XRD patterns of palladium were recorded for all solids between 10 and 100° 2θ using the same equipment.

Elemental analysis. S contents of the silica was determined by Inductively Coupled Plasma-Atomic Emission Spectroscopy (ICP-AES) using a Metrohm IC Plus 883. Pd contents of the solid samples and in the liquids from catalysis experiments were analyzed by Atomic Absorption Spectroscopy (AAS) using an AAS, AANALYST200 Perkin Elmer.

Results and discussion

The nitrogen sorption isotherms of the synthesized silica materials are type IV following the IUPAC classification (Fig. 1A) since they show one step capillary condensation in the adsorption branch, corresponding to the filling of the uniform mesoporous by N_2 molecules. The isotherm shows a typical parallel hysteresis of the open mesopores of SBA-15. In the case of plugged SBA-15, which consists of well-ordered mesoporous silica with constrictions and nanocavities in the pores, N_2 physisorption showed an ink-bottle hysteresis typical for cage-like materials, where desorption is delayed until P/P_o is around 0.47. For the m-MCF material, the isotherms showed a broader ink-bottle hysteresis compared to P-SBA-15, confirming the larger cavities inside this material (22 nm in the case of m-MCF and 6 nm for P-SBA-15).

Argon physisorption at 77 K is an alternative method to study the entrance size of these materials due to the capillary evaporation which occurs at lower relative pressures, extending its use to analyze smaller entrance sizes. Ar physisorption of plugged SBA-15 and m-MCF (ESI,† Fig. S1) showed that the entrance size of the cavities had a broad size distribution from 5.6 to 3.6 nm in the case of P-SBA-15 and all entrance sizes were smaller than 3.6 nm for m-MCF.

The thiol groups were grafted on the surface of silica materials using a post synthetic procedure (Scheme 1). Fig. 1B shows the isotherms for N_2 physisorption of materials after thiol functionalization. It is observed that functionalized samples displayed a decrease in the specific surface area (Table S1†) and pore volume, suggesting the functionalization of the internal and probably of the external walls of OMS

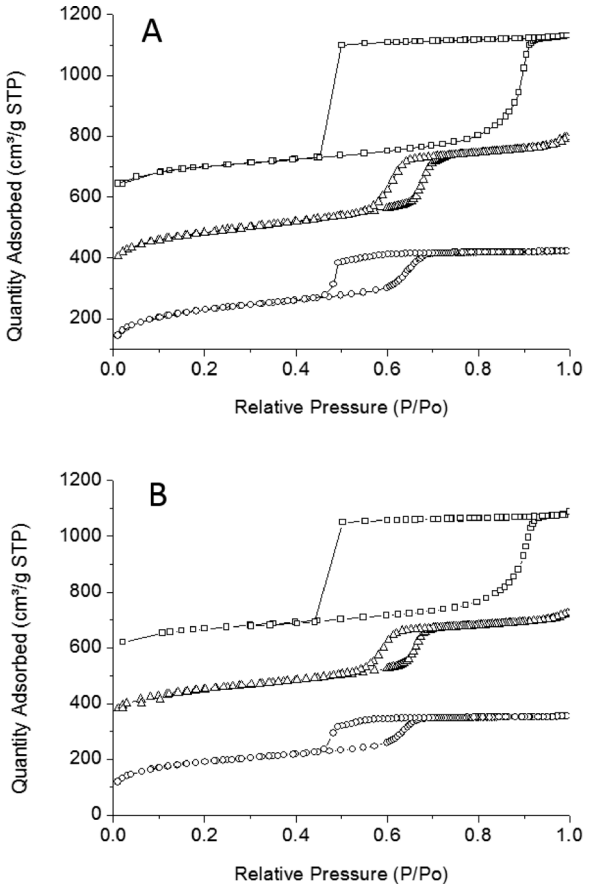

Fig. 1 Nitrogen physisorption of ordered mesoporous silica (A) and functionalized ordered mesoporous materials (B). The isotherms were offset by 300 $cm^3\ g^{-1}$ (SBA-15) and 500 $cm^3\ g^{-1}$ (m-MCF).

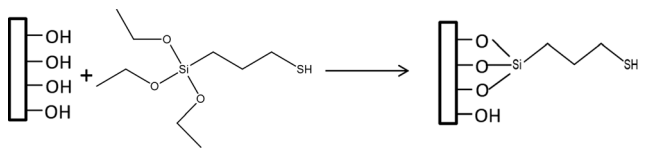

Scheme 1 Functionalization of silica surface with thiol groups.

materials. The same phenomena were observed for Aerosil samples (designation SiO_2); silica composed of spheres packed together (N_2 physisorption in Fig. S2†). In the case of SiO_2, two different methodologies were used (Table 1, designated after Pd loading as SiO_2-SHPd and SiO_2-aSHPd), allowing to obtain materials with different thiol loadings.

SEM images (Fig. S3†) showed no changes in the morphology after the functionalization procedure. STEM-HAADF analysis (Fig. 2) showed that the materials kept the same regularity in pore structure. The open pore structure of SBA-15, the constrictions and nanocavities inside plugged SBA-15 and the cages of m-MCF are shown in Fig. 2A–C, respectively.

After the synthesis of the hybrid supports, palladium was deposited on functionalized silica using a methodology described recently by our group.[62] TEM analysis (Fig. 3) showed that for all cases the structure of silica was unchanged and Pd particles with a very narrow size distribution were observed with an average size of 2.0 ± 0.5 nm. This facilitates the comparison of the catalytic performance of the materials while excluding the influence of the particle size. Table 1 shows the structural properties of the obtained materials. XRD patterns of the fresh catalysts are shown in Fig. S4† showing a very broad peak around $2\theta = 50°$ from which we could not derive a crystallite size.

The Heck reaction

Table 2 shows the conversion for the Heck reaction between iodobenzene and butyl acrylate (Scheme 2) and the Pd leached after the separation of the catalysts; in all cases butyl cinnamate was the only product formed, the conversion of bromide and chloride substrates are shown in Table S2.† All OMS-based catalysts gave rise to similar conversion and metal leaching. However, SiO_2-SHPd showed a slightly higher metal leaching. Please note that a mixture of solvents (toluene + DMF) was used as previously reported.[62]

The loading of thiol groups on the surface of Aerosil was increased, provided that it had the same thiol loading and molar ratio between Pd and S as those of OMS materials (SiO_2-aSHPd, Table 1). However, this sample showed almost no activity, probably caused by the over-coordination of palladium. As Aerosil has a lower specific surface area, the density of thiol per m^2 was much higher (Table 1); this fact might be the reason causing the poisoning of the Pd species. Moreover, Pd leaching was lower for this solid compared to that for OMS, indicating a stronger interaction between Pd and the ligands on this material. This result is in agreement with an earlier report by Jones *et al.*,[64] that an excess of thiol groups was able to poison Pd species, resulting in a loss of activity for the Heck reaction.

The hot filtration test and PVP test were used to investigate the nature of the reactive species, *i.e.*, surface or leached Pd (Table S3†). In all cases, hot filtration showed that leached metal species had a strong influence on the activity for the Heck reaction. Moreover, when PVPy was added, the

Table 1 Structure and composition of silica supported Pd catalysts

Material	Surface area ($m^2\ g^{-1}$)	Pore volume ($cm^3\ g^{-1}$)	S loading (w/w%)	SH density (μmol m^{-2})	Pd loading (w/w%)	S : Pd molar ratio
SiO_2-SHPd	280	2.32	1.2	1.3	1.48	2.7
SiO_2-aSHPd	210	1.47	2.5	3.7	1.54	5.4
SBA-15SHPd	660	0.53	2.7	1.3	1.6	5.6
P.SBA-15SHPd	619	0.52	2.43	1.2	1.55	5.2
m-MCF-SHPd	534	0.72	2.61	1.5	1.57	5.5

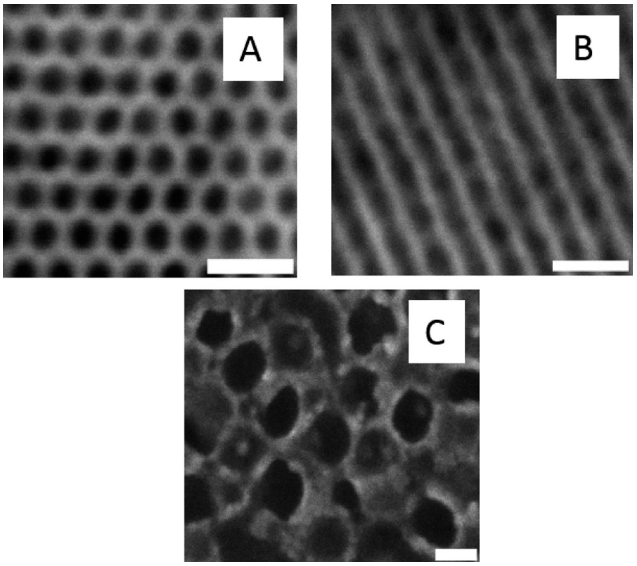

Fig. 2 STEM-HAAD images of (A) SBA-15 SH, (B) P-SBA-15 SH and (C) m-MCF SH. Scale bars: 20 nm.

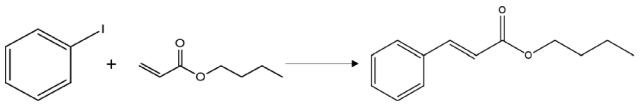

Scheme 2 The Heck reaction between iodobenzene and butyl acrylate.

Table 2 The catalytic performance of all synthesized materials and the Pd leaching after the Heck reaction[a]

Samples	Conversion (%)	Pd leaching (%)
SBA-15SHPd	88	0.8
P-SBA-SHPd	88	0.9
m-MCF-SHPd	89	0.7
SiO_2-SHPd	85	2.4
SiO_2-aSHPd	5	—

[a] Reaction conditions: 2.25 mmol of iodobenzene, 3.4 mmol of butyl acrylate, 20 mg of supported catalyst (0.1 mol% palladium), 2.14 mmol of Et_3N, 2.0 mL of toluene + 0.2 mL of DMF, 100 °C, 12 hours reaction time.

conversion dropped tremendously, confirming the results obtained for the hot filtration tests. This fact might explain why all fresh materials with the same density of thiol displayed almost the same reaction rate (Fig. S5, ESI†).

The recyclability of the catalysts is shown in Fig. 4; a commercial Pd/C catalyst, one of the most used catalysts for these reactions, was also used to compare its stability with those of the synthesized materials. In the case of Pd/C, the catalyst suffered from high metal leaching (20% of the original Pd amount); as a consequence, no conversion was observed after three cycles, showing the limited stability of this material for the Heck reaction under applied conditions. SiO_2-SHPd started to face a considerable decrease in activity after four cycles, however, this catalyst showed a higher stability than Pd/C. The solids based on OMS could be used 7 times with only a slight reduction of the activity, in line with an earlier publication.[62] However, here it is shown that Pd on OMS is more stable than Pd on activated carbon or non-porous silica (Aerosil).

Fig. 5 shows conversion *versus* time plots of the fresh and spent catalysts after four cycles for P.SBA-15SHPd and SiO_2-SHPd. The experiments were run at a lower palladium concentration (0.01 mol% Pd related to iodobenzene). In the case of P.SBA-15SHPd, almost the same reaction rate for fresh and spent catalysts is noted. However, the SiO_2-SHPd sample displayed a considerable decrease of reaction rate for the spent catalyst. To reveal the reason for deactivation, the

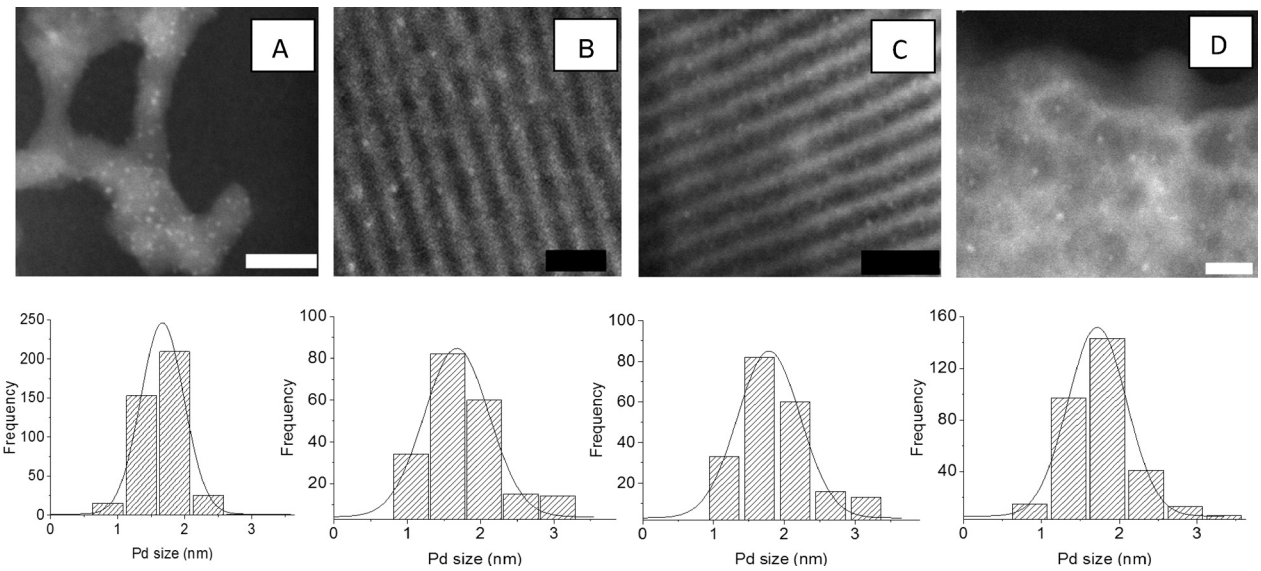

Fig. 3 TEM images of (A) SiO_2-SHPd (B) SBA-15SHPd (C) P.SBA-15SHPd (D) m-MCF-SHPd and the corresponding histograms on the bottom. Scale bars are 20 nm.

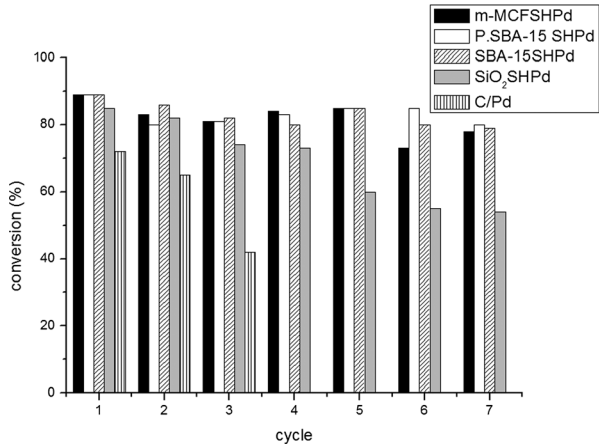

Fig. 4 Recyclability of synthesized materials for the Heck reaction. Reaction conditions: 2.25 mmol of iodobenzene, 3.4 mmol of butyl acrylate, 20 mg of supported catalyst (0.13 mol% palladium), 2.14 mmol of base, 2.0 mL of toluene + 0.2 mL of DMF, 100 °C, 12 hours (toluene + DMF).

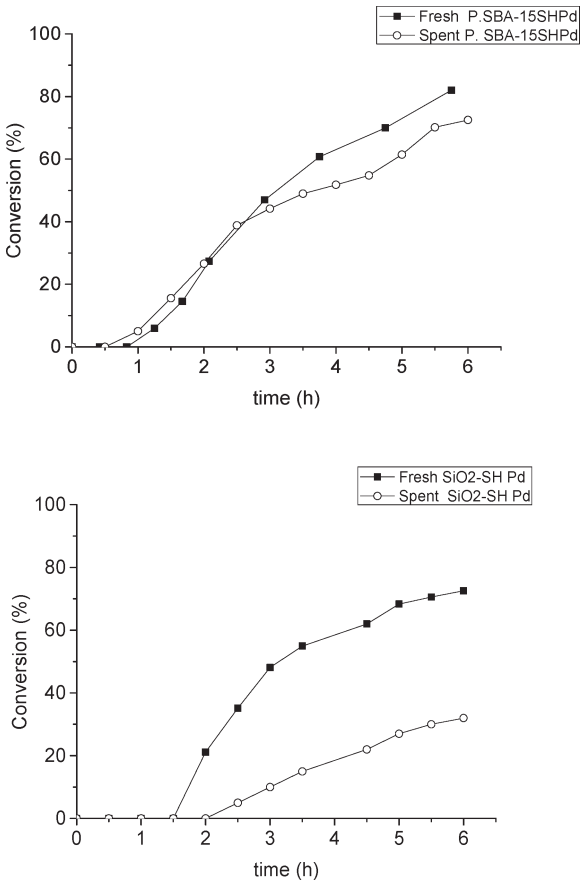

Fig. 5 Plot of product yield *versus* time for the Heck reaction with fresh and spent (after four previous reaction cycles) SiO_2-SHPd and P.SBA-15SHPd. Reaction conditions: 22.5 mmol of iodobenzene, 34 mmol of butyl acrylate, 20 mg of supported catalyst (0.01 mol% palladium), 21.4 mmol of Et_3N, 20 mL of toluene + 2 mL of DMF, 100 °C.

spent catalysts (after four cycles) were studied by X-ray diffraction (XRD) and transmission electron microscopy (TEM). XRD analysis (Fig. S4†) showed new lines due to changes in enhanced palladium crystallinity for all catalysts; the new pattern lines corresponded to the Pd metal with a face-centered cubic structure. These results differ from those obtained by Shimizu *et al.*[65] who reported no change in palladium crystallinity after the C–C cross coupling reaction using FDU as a support. The obtained results give a strong indication that during the catalytic reaction the palladium species leached into the solution and were re-deposited on the silica surface, leading to particle growth (Ostwald ripening) and enhanced crystallinity of Pd.

TEM analyses of the spent catalysts and histograms of Pd particle size distribution (after 4 cycles) are shown in Fig. 6. The structures of plugged SBA-15 and m-MCF were still recognized, but the palladium particle size had grown slightly, and the majority of metal particles were still found to be confined in the silica pore structure (Fig. 6B, C). In the case of SiO_2-SHPd, particles grew severely (Fig. 6A), and very large metal particles from 10–160 nm in diameter were found on the external surface of the silica aggregates. These results give a strong indication that the combination of thiol groups and confinement of Pd particles in mesopores had restricted the Pd growth in the case of P.SBA-15 and m-MCF, producing more stable catalysts than SiO_2-SHPd where confinement effects were limited. The fact that the great majority of the particles of spent m-MCF-SHPd are smaller than particles of spent P-SBA-15SHPd might be related to the small window size of m-MCF limiting the Ostwald ripening.

As shown by hot filtration and PVP tests, Pd species leached from the support and brought about the catalytic process in solution. Thus, the recapturing process is very important to reduce the formation of large particles and to extend the catalyst lifetime. Despite having the same density of thiol groups per unit of surface area, the Pd particles grew much more severely on Aerosil; we think that the mesopores of OMS provide a concave surface structure with more effective functionalization, and moreover, the confinement of Pd nanoparticles helps to re-adsorb Pd species and thereby decrease the palladium particle growth. In the case of Aerosil, the convex surface structure may provide less effective functionalization, on the one hand, and the fact that Pd nanoparticles are not effectively confined inside pores results in the faster growth of Pd particles *via* Ostwald ripening, on the other hand.

The porosity of the spent catalysts was also investigated by N_2 physisorption to examine the stability of OMS under Heck reaction conditions (Fig. S6†). Isotherms of fresh and spent catalysts showed that the support materials kept almost the same porosity after 4 cycles, showing no damage to the silica structure under the applied conditions.

The Suzuki reaction

The reaction between 4-iodoanisole and phenylboronic acid was used as a model reaction (Scheme 3). Table 3 shows the

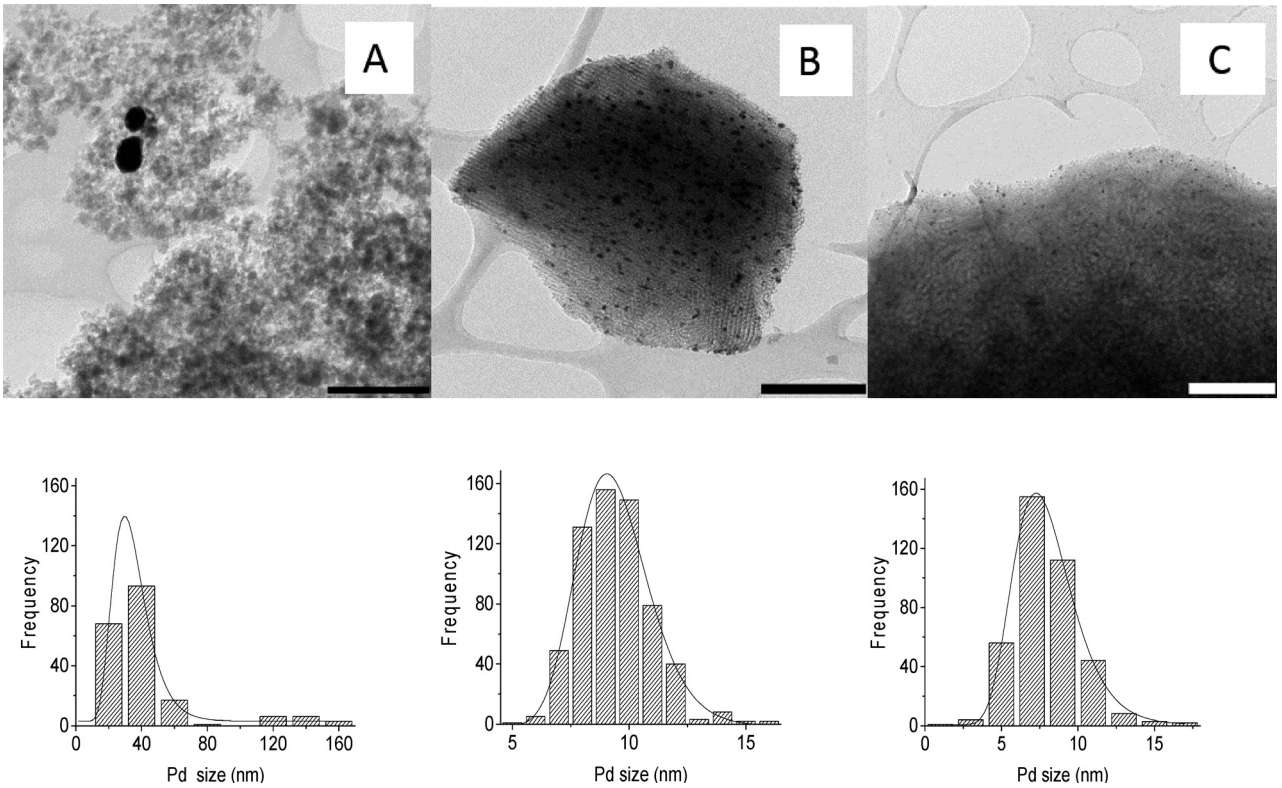

Fig. 6 TEM images of spent catalysts after the 4th cycle: (A) SiO_2-SHPd, (B) P.SBA-15SHPd and (C) m-MCF-SHPd (scale bars: 200 nm) and derived Pd particle size distributions.

performance of P.SBA-15SHPd when different solvents and bases were used. In the case of the Suzuki reaction, Et_3N was found to be inefficient when compared to $Na_3PO_4{\cdot}12H_2O$ and K_2CO_3. Anhydrous Na_3PO_4 was also used as a base, but a lower conversion was observed, indicating the influence of water on this reaction as reported before.[66] Moreover, ethanol was found to be a better solvent compared to pure DMF and a mixture of DMF and toluene. The conversion of bromide and chloride substrates is shown in Table S4.†

The recyclability test of the catalysts was carried out using the conditions described in Table 3 entry 7. The commercial Pd/C catalyst was used to compare its performance with the silica-supported catalysts. All catalysts suffered a considerable deactivation after each cycle (Fig. 7). SBA-15SHPd suffered the strongest deactivation when compared to the other materials. As observed for the Heck reaction, Pd/C suffered again from severe leaching, leading a short lifetime.

The stability of the supports was examined to address a possible explanation for this extensive deactivation. Fig. 8 shows the low angle XRD patterns of the spent (1 cycle) P.SBA-15SHPd and SBA-15SHPd. The peaks which correspond to the *p6mm* configuration are not detected for SBA-15, indicating that the pores had collapsed during catalysis. Probably the alkaline conditions applied during the Suzuki reaction were responsible for the pore collapse. Plugged SBA-15 preserved its structure after the first cycle (Fig. 8) as the peaks which correspond to the pore configuration were still visible. This is a clear indication of the higher stability of P-SBA-15 when compared to SBA-15 due to its robust structure and wall thickness. TEM was also used to confirm these results; no well-structured pores were observed on the spent SBA-15 sample, and on the other hand, the pore structure was still observed for P-SBA-15 (Fig. S7†).

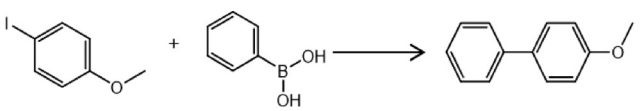

Scheme 3 The Suzuki reaction between 4-iodoanisole and phenylboronic acid.

Table 3 Results of the Suzuki reaction of 4-iodoanisole and phenylboronic acid using different bases and solvents for P.SBA-15SHPd

Entry	Solvent	Base	Conversion (%)	T (°C)
1[a]	DMF/toluene	Et_3N	2	100
2	DMF	Et_3N	8	100
3	Ethanol	Et_3N	5	60
4	Ethanol	*n*-Butylamine	7	60
5	DMF	$Na_3PO_4{\cdot}12H_2O$	30	60
6	DMF/toluene	$Na_3PO_4{\cdot}12H_2O$	21	60
7	Ethanol	$Na_3PO_4{\cdot}12H_2O$	80	60
8	Ethanol	K_2CO_3	41	60
9	Ethanol	Na_3PO_4	45	60

Conditions: 4-iodoanisole (2.4 mmol), phenylboronic acid (2.88 mmol), base (2.4 mmol), 20 mg of P.SBA-15SHPd (0.12 mol% Pd), 3 hours.[a] 12 hours.

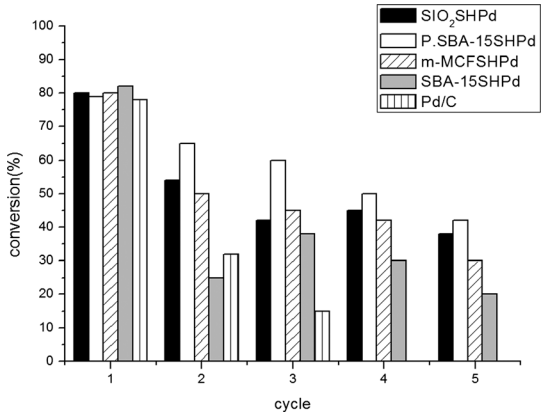

Fig. 7 Recyclability of synthesized materials for the Suzuki reaction. Conditions: 4-iodoanisole (2.4 mmol), phenylboronic acid (2.88 mmol), $Na_3PO_4{\cdot}12H_2O$ (2.4 mmol), around 20 mg of catalyst (0.12 mol% Pd), 70 °C, 3 hours.

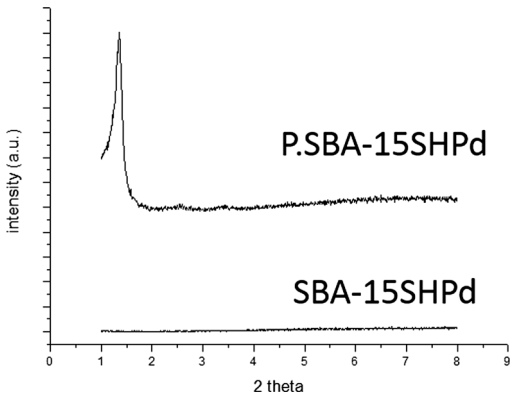

Fig. 8 Low angle XRD of SBA-15SHPd and P.SBA-15SHPd used for the Suzuki reaction (after the 1st cycle).

The porosity of the spent materials after the first cycle was also investigated by N_2 physisorption (isotherms in the ESI,† Fig. S8); all materials faced a strong loss of surface area and pore volume (Table 4). However, plugged SBA-15 was found to be a more resistant material compared to the other mesoporous materials SBA-15 and m-MCF. In the case of P-SBA-15, the surface area decreased but not as severe as those for SBA-15 and m-MCF; a clear ink-bottle hysteresis could still be seen (ESI,† Fig. S8).This can also explain the higher metal leaching from SBA-15SHPd when compared to those from SiO_2-SHPd and P.SBA-15SHPd (Table 4). Probably the destruction of the pores resulted in the reduction of the accessibility of the thiol groups, as a consequence limiting the recovery of the palladium species by the ligands. It is also interesting to point out that P.SBA-15SHPd showed the best recyclability when compared to the other studied supports (Fig. 7). For the Suzuki reaction, the collapse of the silica structure might be considered as the main factor contributing to the deactivation of silica-based catalysts. As shown in Table 4, SBA-15 lost 24% of the Pd originally deposited on SBA-15; however, the catalyst suffered a larger reduction in activity after the first cycle (from 80% to 26%) which cannot be just explained just by leaching.

Conclusion

In summary, the structural stability of Pd species was influenced by the thiol-functionalized silica structure. Here, we report for the first time that for the Heck reaction, the combined effects of functionalization and confinement of Pd nanoparticles in the cavities of ordered mesoporous silica P-SBA-15 or m-MCF were efficient to limit the Ostwald ripening avoiding the formation of large Pd particles that was observed with non-porous silica. Despite having the same Pd particle size distribution, the materials based on OMS showed a better recyclability when compared to non-porous silica due to the prevention of the formation of large Pd particles. The hot filtration and PVP tests showed that homogeneous species contributed considerably to the final conversion. Stabilization of the heterogeneous Heck Pd catalyst, therefore, cannot be realized by suppression of leaching. Rather, re-adsorption by functionalization in combination with restriction of Pd particle growth by confinement is effective to extend the catalyst lifetime.

In the case of the Suzuki reaction, the use of stronger alkaline conditions promotes considerable damage to silica supports. This fact resulted in the limited recyclability of all synthesized materials. However, SBA-15 was found to be the most fragile structure, which collapsed during the first cycle, resulting in a poor recyclability when compared to P-SBA-15. The plugs and the most robust structure of P-SBA-15 permitted the material to display a higher stability for the Suzuki reaction, providing an improvement of the recyclability results.

Table 4 Structural characteristics of catalysts for the Suzuki reaction after the 1st cycle

Material	BET surface area ($m^2\ g^{-1}$)	Pore volume ($cm^3\ g^{-1}$)	Pd leaching[a] (%)
SBA-15 SHPd	15	0.004	24
P.SBA-15SHPd	154	0.16	5
m-MCF-SHPd	50	0.07	15
SiO_2-SHPd	100	0.16	6

[a] Based on the original amount of Pd deposited on the silica structure.

Acknowledgements

The authors acknowledge support from European Research Council (ERC) advanced grant no. 338846 and the Dutch National Research School Combination Catalysis (NRSCC).

References

1 L.-L. Li, H. Sun, C.-J. Fang, J. Xu, J.-Y. Jin and C.-H. Yan, *J. Mater. Chem.*, 2007, **17**, 4492.
2 R. Métivier, I. Leray, B. Lebeau and B. Valeur, *J. Mater. Chem.*, 2005, **15**, 2965.
3 D.-H. Lin, Y.-X. Jiang, Y. Wang and S.-G. Sun, *J. Nanomater.*, 2008, **2008**, 1.
4 S. Wang, *Microporous Mesoporous Mater.*, 2009, **117**, 1.
5 I. I. Slowing, J. L. Vivero-Escoto, C.-W. Wu and V. S.-Y. Lin, *Adv. Drug Delivery Rev.*, 2008, **60**, 1278.
6 M. Vallet-Regí, F. Balas and D. Arcos, *Angew. Chem., Int. Ed.*, 2007, **46**, 7548.
7 X. Liu, L. Li, Y. Du, Z. Guo, T. T. Ong, Y. Chen, S. C. Ng and Y. Yang, *J. Chromatogr. A*, 2009, **1216**, 7767.
8 H. Wan, L. Liu, C. Li, X. Xue and X. Liang, *J. Colloid Interface Sci.*, 2009, **337**, 420.
9 L. Escamilla-Perea, R. Nava, B. Pawelec, M. G. Rosmaninho, C. L. Peza-Ledesma and J. L. G. Fierro, *Appl. Catal., A*, 2010, **381**, 42.
10 H. Yang, L. Zhang, W. Su, Q. Yang and C. Li, *J. Catal.*, 2007, **248**, 204.
11 T.-W. Kim, M.-J. Kim, F. Kleitz, M. M. Nair, R. Guillet-Nicolas, K.-E. Jeong, H.-J. Chae, C.-U. Kim and S.-Y. Jeong, *ChemCatChem*, 2012, **4**, 687.
12 M. Shakeri, R. J. M. Klein Gebbink, P. E. de Jongh and K. P. de Jong, *Angew. Chem.*, 2013, **125**, 11054.
13 M. C. G. Albuquerque, I. Jiménez-Urbistondo, J. Santamaría-González, J. M. Mérida-Robles, R. Moreno-Tost, E. Rodríguez-Castellón, A. Jiménez-López, D. C. S. Azevedo, C. L. Cavalcante Jr. and P. Maireles-Torres, *Appl. Catal., A*, 2008, **334**, 35.
14 S. Das, A. Goswami, N. Murali and T. Asefa, *ChemCatChem*, 2013, **5**, 910.
15 A. Taguchi and F. Schüth, *Microporous Mesoporous Mater.*, 2005, **77**, 1.
16 Y.-S. Kim, X.-F. Guo and G.-J. Kim, *Chem. Commun.*, 2009, 4296.
17 H. Yang, L. Zhang, P. Wang, Q. Yang and C. Li, *Green Chem.*, 2009, **11**, 257.
18 H. Yang, X. Han, Z. Ma, R. Wang, J. Liu and X. Ji, *Green Chem.*, 2010, **12**, 441.
19 S.-Y. Chen, T. Yokoi, C.-Y. Tang, L.-Y. Jang, T. Tatsumi, J. C. C. Chan and S. Cheng, *Green Chem.*, 2011, **13**, 2920.
20 J. Fan, X. Jiang, H. Min, D. Li, X. Ran, L. Zou, Y. Sun, W. Li, J. Yang, W. Teng, G. Li and D. Zhao, *J. Mater. Chem. A*, 2014, **2**, 10654.
21 R. L. Oliveira, P. K. Kiyohara and L. M. Rossi, *Green Chem.*, 2010, **12**, 144.
22 R. L. Oliveira, P. K. Kiyohara and L. M. Rossi, *Green Chem.*, 2009, **11**, 1366.
23 Z. Wang, Q. Liu, J. Yu, T. Wu and G. Wang, *Appl. Catal., A*, 2003, **239**, 87.
24 E. M. Fixman, M. C. Abello, O. F. Gorriz and L. A. Arrúa, *Appl. Catal., A*, 2007, **319**, 111.
25 Z. Huang, F. Cui, H. Kang, J. Chen, X. Zhang and C. Xia, *Chem. Mater.*, 2008, **20**, 5090.
26 R. L. Oliveira, D. Zanchet, P. K. Kiyohara and L. M. Rossi, *Chemistry*, 2011, **17**, 4626.
27 Y. Hao, Y. Chong, S. Li and H. Yang, *J. Phys. Chem. C*, 2012, **116**, 6512.
28 G. Prieto, M. Shakeri, K. P. de Jong and P. E. de Jongh, *ACS Nano*, 2014, **8**, 2522.
29 J. Sun, D. Ma, H. Zhang, X. Liu, X. Han, X. Bao, G. Weinberg, N. Pfänder and D. Su, *J. Am. Chem. Soc.*, 2006, **128**, 15756.
30 J. M. Kisler, M. L. Gee, G. W. Stevens and A. J. O. Connor, *Chem. Mater.*, 2003, **15**, 619.
31 H. N. Pham, A. E. Anderson, R. L. Johnson, K. Schmidt-Rohr and A. K. Datye, *Angew. Chem., Int. Ed.*, 2012, **51**, 13163.
32 P. Van Der Voort, P. I. Ravikovitch, K. P. De Jong, M. Benjelloun, E. Van Bavel, A. H. Janssen, A. V. Neimark, B. M. Weckhuysen and E. F. Vansant, *J. Phys. Chem. B*, 2002, **123**, 5873.
33 P. Van der Voort, P. I. Ravikovitch, K. P. De Jong, A. V. Neimark, A. H. Janssen, M. Benjelloun, E. Van Bavel, P. Cool, B. M. Weckhuysen and E. F. Vansant, *Chem. Commun.*, 2002, 1010.
34 E. B. Celer, M. Kruk, Y. Zuzek and M. Jaroniec, *J. Mater. Chem.*, 2006, **16**, 2824.
35 M. Shakeri, R. J. M. Klein Gebbink, P. E. de Jongh and K. P. de Jong, *Microporous Mesoporous Mater.*, 2013, **170**, 340.
36 R. L. Oliveira, M. Shakeri, J. D. Meeldijk, K. P. de Jong and P. E. de Jongh, *Microporous Mesoporous Mater.*, 2015, **201**, 234.
37 M. Shakeri, L. Roiban, V. Yazerski, G. Prieto, J. M. K. Gebbink, P. E. De Jongh and K. P. De Jong, *ACS Catal.*, 2014, **4**, 3791.
38 F. Yin, S. Ji, P. Wu, F. Zhao and C. Li, *J. Catal.*, 2008, **257**, 108.
39 B. Karimi, S. Abedi, J. H. Clark and V. Budarin, *Angew. Chem., Int. Ed.*, 2006, **45**, 4776.
40 X. Zhang, H. Yin, J. Wang, L. Chang, Y. Gao, W. Liu and Z. Tang, *Nanoscale*, 2013, **5**, 8392.
41 G. Chen, S. Wu, H. Liu, H. Jiang and Y. Li, *Green Chem.*, 2013, **15**, 230–235.
42 P. M. Ulberman, N. J. S. Costa, K. Philippot, R. C. Carmona, A. A. dos Santos and L. M. Rossi, *Green Chem.*, 2014, **16**, 4566.
43 T. Ishida, Y. Onuma, K. Kinjo, A. Hamasaki, H. Ohashi, T. Honma, T. Akita, T. Yokoyama, M. Tokunaga and M. Haruta, *Tetrahedron*, 2014, **70**, 6150.
44 D. D. L. Martins, H. M. Alvarez, L. C. S. Aguiar and O. A. C. Antunes, *Appl. Catal., A*, 2011, **408**, 47.
45 N. J. S. Costa, P. K. Kiyohara, A. L. Monteiro, Y. Coppel, K. Philippot and L. M. Rossi, *J. Catal.*, 2010, **276**, 382.

46 D. Das and A. Sayari, *J. Catal.*, 2007, **246**, 60.
47 A. Gruber, D. Zim, G. Ebeling, A. Monteiro and J. Dupont, *Org. Lett.*, 2000, **2**, 1287.
48 K. Köhler, R. G. Heidenreich, J. G. E. Krauter and J. Pietsch, *Chemistry*, 2002, **8**, 622.
49 G. Zhang, H. Zhou, J. Hu, M. Liu and Y. Kuang, *Green Chem.*, 2009, **11**, 1428.
50 B. Nohair, S. Macquarrie, C. M. Crudden and S. Kaliaguine, *J. Phys. Chem. C*, 2008, **112**, 6065.
51 S. Macquarrie, B. Nohair, J. H. Horton, S. Kaliaguine and C. M. Crudden, *J. Phys. Chem. C*, 2010, **114**, 57.
52 M. Pagliaro, V. Pandarus, F. Béland, R. Ciriminna, G. Palmisano and P. D. Carà, *Catal. Sci. Technol.*, 2011, **1**, 736.
53 G. Budroni, A. Corma, H. Garcia and A. Primo, *J. Catal.*, 2007, **251**, 345.
54 G. Park, S. Lee, S. J. Son and S. Shin, *Green Chem.*, 2013, **15**, 3468.
55 J. H. Clark, D. J. Macquarrie and E. B. Mubofu, *Green Chem.*, 2000, **2**, 53.
56 B. Karimi and D. Enders, *Org. Lett.*, 2006, **8**, 1237.
57 V. Polshettiwar and Á. Molnár, *Tetrahedron*, 2007, **63**, 6949.
58 D. Zhang, J. Xu, Q. Zhao, T. Cheng and G. Liu, *ChemCatChem*, 2014, **10**, 2998.
59 A. El Kadib, K. McEleney, T. Seki, T. K. Wood and C. M. Crudden, *ChemCatChem*, 2011, **3**, 1281.
60 L. Wang, S. Shylesh, D. Dehe, T. Philippi, G. Dörr, A. Seifert, Z. Zhou, M. Hartmann, R. N. Klupp Taylor, M. Jia, S. Ernst and W. R. Thiel, *ChemCatChem*, 2012, **4**, 395.
61 L. M. Rossi, L. L. R. Vono, F. P. Silva, P. K. Kiyohara, E. L. Duarte and J. R. Matos, *Appl. Catal., A*, 2007, **330**, 139.
62 R. L. Oliveira, J. B. F. Hooijmans, P. E. deJongh, R. J. M. Klein Gebbink and K. P. de Jong, *ChemCatChem*, 2014, **6**, 3223.
63 X. Ma, Y. Zhou, J. Zhang, A. Zhu, T. Jiang and B. Han, *Green Chem.*, 2008, **10**, 59.
64 J. Richardson and C. Jones, *J. Catal.*, 2007, **251**, 80.
65 K. Shimizu, S. Koizumi, T. Hatamachi, H. Yoshida, S. Komai, T. Kodama and Y. Kitayama, *J. Catal.*, 2004, **228**, 141.
66 J. Webb, S. Macquarrie, K. Mceleney and C. Crudden, *J. Catal.*, 2007, **252**, 97.

